J. Fluid Mech. (2013), *vol.* 714, *pp.* 336–360.
doi:10.1017/jfm.2012.480

Coupled oscillations of deformable spherical-cap droplets. Part 2. Viscous motions

J. B. Bostwick[1,2] **and P. H. Steen**[2,3,†]

[1]Department of Mathematics, North Carolina State University, Raleigh, NC 27695, USA

[2]Department of Theoretical & Applied Mechanics, Cornell University, Ithaca, NY 14853, USA

[3]School of Chemical and Biomolecular Engineering and Center for Applied Mathematics, Cornell University, Ithaca, NY 14853, USA

(Received 6 April 2012; revised 7 August 2012; accepted 21 September 2012)

A spherical drop is constrained by a solid support arranged as a latitudinal belt. The spherical belt splits the drop into two deformable spherical caps. The edges of the belt support are given by lower and upper latitudes, yielding a support of prescribed extent and position: a two-parameter family of geometrical constraints. In this paper we study the linear oscillations of the two coupled surfaces in the viscous case, the inviscid case having been dealt with in Part 1 (Bostwick & Steen, *J. Fluid Mech.*, vol. 714, 2013, pp. 312–335), restricting to axisymmetric disturbances. For the viscous case, limiting geometries are the spherical-bowl constraint of Strani & Sabetta (*J. Fluid Mech.*, vol. 189, 1988, pp. 397–421) and free viscous drop of Prosperetti (*J. Méc.*, vol. 19, 1980*b*, pp. 149–182). In this paper, a boundary-integral approach leads to an integro-differential boundary-value problem governing the interface disturbances, where the constraint is incorporated into the function space. Viscous effects arise due to relative internal motions and to the no-slip boundary condition on the support surface. No-slip is incorporated using a modified set of shear boundary conditions. The eigenvalue problem is then reduced to a truncated set of algebraic equations using a spectral method in the standard way. Limiting cases recover literature results to validate the proposed modification. Complex frequencies, as they depend upon the viscosity parameter and the support geometry, are reported for both the drop and bubble cases. Finally, for the drop, an approximate boundary between over- and under-damped motions is mapped over the constraint parameter plane.

Key words: bubble dynamics, capillary flows, drops

1. Introduction

Since early studies of capillarity (Segner 1751; Maxwell 1898), the restorative force of surface tension has been compared to that of an elastic body. Surface tension resists deformation of a liquid mass from rest configurations in much the same way as the linear-elastic spring resists excursions of a mass from a rest position. Indeed, under broad conditions, the linear stability of a liquid mass held by surface tension is determined by an operator equation on small disturbances to the interface of the same

† Email address for correspondence: phs7@cornell.edu

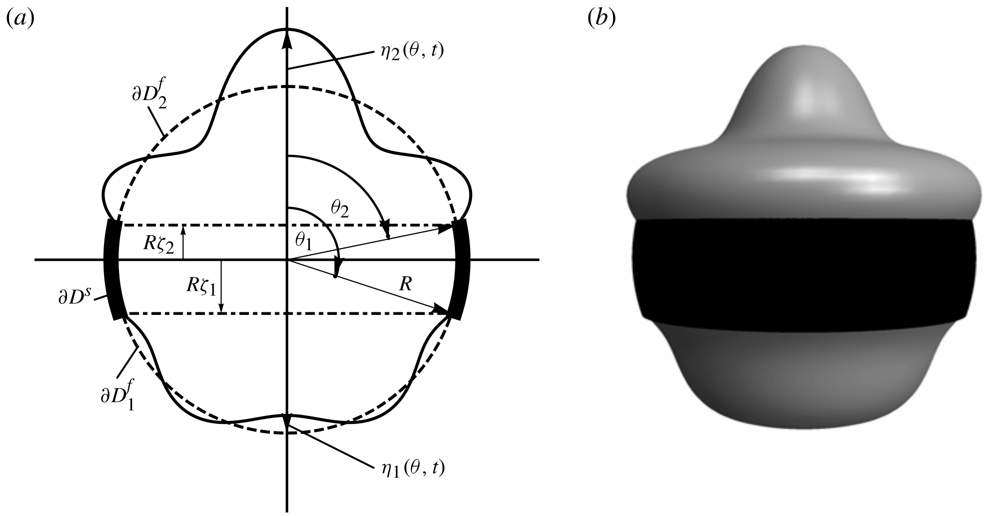

FIGURE 1. (*a*) Definition sketch in two-dimensional polar view and (*b*) sample deformation in three-dimensional perspective view. Disturbances η_1 and η_2 are constrained by the belt support extending over $\zeta_1 \equiv \cos\theta_1 \leqslant \cos\theta \leqslant \zeta_2 \equiv \cos\theta_2$. Lengths ζ are scaled by R while lengths η are left unscaled.

form as that of the characteristic equation for the damped harmonic oscillator,

$$\gamma^2 M + \gamma \varPhi + K = 0. \tag{1.1}$$

Here, γ is the growth rate, M is the disturbance kinetic-energy operator, $\varPhi$ is the disturbance dissipation operator and K the disturbance surface-energy operator. The kinetic energy M is positive definite and the dissipation $\varPhi$ a negative-definite operator that depends on γ in general. The surface energy K can have either sign depending on the nature of the equilibrium configuration. The equilibria are extremals of a corresponding surface-energy functional. For the case of an inviscid liquid drop (Rayleigh problem), the flow is without dissipation $\varPhi = 0$ and K is positive definite, so that schematically $\gamma^2 = -K/M$ and disturbances neither grow nor decay, $\gamma = \pm \mathrm{i}\omega$. Rayleigh (1879) (also Lamb 1932) used normal modes to solve for the operators in (1.1) and to find that the inviscid drop oscillates with frequencies

$$\omega_n^2 = \frac{n(n-1)(n+1)(n+2)}{(n+1)\rho_i + n\rho_e} \frac{\sigma}{R^3}, \quad n = 0, 1, 2, \ldots, \tag{1.2}$$

where σ is the surface tension and ρ_i and ρ_e are the densities of the interior and exterior fluids, respectively. Corresponding mode shapes have radial deformations that are given by the Legendre polynomials, $P_n(\cos\theta)$. Rayleigh's predictions have been verified experimentally for immiscible drops by Trinh, Zwern & Wang (1982) and Trinh & Wang (1982) and for free drops in microgravity by Wang, Anilkumar & Lee (1996). For drops with viscosity (Chandrasekhar 1961; Miller & Scriven 1968; Prosperetti 1980*b*) or moving contact lines (Davis 1980), $\varPhi \neq 0$, and the growth rates typically have real parts so that disturbances can grow or decay. When decay happens, it can occur in an under-damped or over-damped fashion, of course.

In this paper, we study the linear stability of two coupled spherical-cap surfaces made by constraining a spherical drop with a solid support (figure 1). The solid support conforms to the spherical surface and extends between two latitudes, $\theta_2 \leqslant \theta \leqslant \theta_1$, forming a spherical belt. The resulting free surface consists of two spherical caps (disconnected) which are coupled through the liquid beneath (connected). The interfaces are pinned at the edges of the belt and no-slip conditions, as appropriate to viscous liquids, are enforced along the belt. Integro-differential equations for the free-surface disturbances are derived.

These operator equations are then solved, restricting to axisymmetric disturbances. The change in boundary conditions from free to fixed along the support is handled by an indicator function. This approach is new, as far as we are aware, and captures the exact dependence of Φ on γ, as well as that of M, Φ and K on the support geometry (θ_1, θ_2), density contrast and a viscosity parameter. This paper (Part 2) focuses on the dependence of the dissipation Φ on viscosity and support geometry, whereas Part 1 (Bostwick & Steen 2013) concerns motions of the surfaces as coupled oscillators driving inviscid flows.

Viscous effects, as they relate to the free drop problem, have been investigated by Reid (1960) for an isolated drop in a vacuum, and Chandrasekhar (1961), who establishes boundaries between under-damped and over-damped motion. Miller & Scriven (1968) have derived a dispersion relationship for immiscible drops, whose interface may or may not have elastic properties. Prosperetti (1980*b*) uses a normal-mode analysis to obtain the spectrum for immiscible viscous drops, results later confirmed computationally by Basaran (1992). As an alternative to normal-mode analysis, Prosperetti (1980*a*,*c*) has studied the initial-value problem and has identified three phases of evolution. The first phase is characterized by irrotational flow, the second phase by diffusion into the bulk of vorticity generated at the drop surface and the final phase by decay of the least-damped normal mode. With regard to large-amplitude behaviour, Smith (2010) uses a strongly nonlinear analysis to derive a set of modulation equations showing that the decay rate for the free drop can be approximated by a quadratic function of the disturbance amplitude. Alternatively, finite-element methods have been employed to study the finite-amplitude natural oscillations of free (Basaran 1992) and pendant (Basaran & DePaoli 1994) drops.

The motions of constrained drops are of interest in a number of emerging applications. Examples include drop atomization (James, Smith & Glezer 2003*a*; James *et al.* 2003*b*; Vukasinovic, Smith & Glezer 2007), switchable electronically controlled capillary adhesion (Vogel, Ehrhard & Steen 2005; Vogel & Steen 2010) and optical microlens devices (López, Lee & Hirsa 2005; López & Hirsa 2008; Olles *et al.* 2011). The last two are rooted in the idea of the capillary switch (Bhandar & Steen 2005; Hirsa *et al.* 2005; Malouin, Vogel & Hirsa 2010). The capillary switch is composed of two disjoint interfaces connected by a tube. The interfaces communicate (coupled) through the underlying fluid, much like the communication that occurs for the belted sphere. The dynamics of the capillary switch for both free (Theisen *et al.* 2007) and forced oscillations (Slater *et al.* 2008) has been studied for centre-of-mass motions, which restricts interface deformations to spherical caps, and for axisymmetric deformations in the limit of zero tube length (Bostwick & Steen 2009). More recently, Ramalingam & Basaran (2010) have analysed the forced oscillations of the double droplet system (DDS) by various types of excitation.

Our solution approach first invokes normal modes and then maps the flow problem (interior domain) onto the undisturbed interface using Green's functions, adopting a boundary-integral approach. This results in an eigenvalue problem of the form of (1.1). More specifically, consider an incompressible, viscous fluid occupying an arbitrary domain D bounded by an interface ∂D held by a constant surface tension σ. The flow is capillarity-driven and governed by the Young–Laplace equation $p/\sigma = 2H$, which relates the pressure jump across the free interface p to its shape through the mean curvature H. In the standard way, time dependence factors out by assuming that field quantities are proportional to

$$\mathrm{e}^{\gamma t}, \tag{1.3}$$

which results in

$$\gamma \boldsymbol{v} = \nabla \cdot \boldsymbol{T}\,[D], \tag{1.4a}$$
$$\nabla \cdot \boldsymbol{v} = 0\,[D], \tag{1.4b}$$
$$\boldsymbol{v} \cdot \boldsymbol{n} = \gamma y\,[\partial D], \tag{1.4c}$$
$$\boldsymbol{T} \cdot \boldsymbol{n} = (2H)_\delta \boldsymbol{n}\,[\partial D], \tag{1.4d}$$

where $\boldsymbol{v}$ is the velocity field, $\boldsymbol{n}$ the surface normal and $(2H)_\delta = (2H)_\delta(y)$ the linearized mean curvature. More specifically, $(2H)_\delta$ is the $O(\delta)$ contribution to the mean curvature of the disturbed equilibrium surface, $\bar{y} \to \bar{y} + \delta y$. Equations (1.4*a*) and (1.4*b*) represent the linearized Navier–Stokes equation and continuity equation for incompressible fluids, respectively. The kinematic condition (1.4*c*) relates the velocity field to the interface disturbance y there. In the case of a velocity potential ϕ for irrotational flow, this reduces to $\partial\phi/\partial n = \gamma y$. Lastly, (1.4*d*) represents the jump in stress across the boundary, where the full stress tensor $\boldsymbol{T}$ is defined in standard notation,

$$\boldsymbol{T} = -p\boldsymbol{1} + \mu \boldsymbol{D}, \tag{1.5a}$$
$$\boldsymbol{D} = \nabla \boldsymbol{v} + (\nabla \boldsymbol{v})^t, \tag{1.5b}$$

with μ the fluid viscosity. Taking the divergence of (1.4*a*) and using (1.4*b*) yields the Laplace equation for the stress tensor. Solving this equation with Green's functions leads to an integro-differential operator on interfacial disturbances y. The no-penetration condition on the solid support is built into the function space while the tangential stress and no-slip boundary conditions remain part of the operator equation. They contribute to the dissipation.

Closely related to the operator equation (1.1) is the energy equation. This functional (mapping functions into the real line) represents a necessary condition on solutions. The energy equation is obtained by taking the dot product of the linearized Navier–Stokes equation (1.4*a*) with $\boldsymbol{v}$,

$$\gamma \int_D |\boldsymbol{v}|^2 = \int_{\partial D} \boldsymbol{v} \cdot \boldsymbol{T} \cdot \boldsymbol{n} - \int_D \nabla \boldsymbol{v} : \boldsymbol{T}. \tag{1.6}$$

The Helmholtz decomposition theorem allows one to decompose the velocity field into a rotational $\boldsymbol{B}$ and irrotational $\nabla\phi$ part (e.g. Batchelor 1967),

$$\boldsymbol{v} = \boldsymbol{B} + \nabla\phi. \tag{1.7}$$

Using this decomposition, one can manipulate the volume integrals of (1.6) into surface integrals,

$$\gamma \int_{\partial D} \phi\, \boldsymbol{v} \cdot \boldsymbol{n} + \mu \int_{\partial D} \boldsymbol{n} \cdot \boldsymbol{D} \cdot (\boldsymbol{v} + \boldsymbol{B}) - \int_{\partial D} (2H)_\delta \boldsymbol{v} \cdot \boldsymbol{n} = 0. \tag{1.8}$$

A further simplification to (1.8) results when the surrounding fluid is a passive gas, which requires the shear stress to vanish at the surface,

$$\int_{\partial D}\left(\gamma^2\phi+\gamma\mu\boldsymbol{n}\cdot\boldsymbol{D}\cdot\boldsymbol{n}\left(1+\frac{\boldsymbol{B}\cdot\boldsymbol{n}}{\boldsymbol{v}\cdot\boldsymbol{n}}\right)-(2H)_\delta\right)y=0. \tag{1.9}$$

Note that (1.9) takes the form of (1.1), with operators replaced by functionals. The functionals M, Φ and K can be read off as

$$M\equiv\int_{\partial D}\phi\, y,\quad \Phi\equiv\mu\int_{\partial D}\boldsymbol{n}\cdot\boldsymbol{D}\cdot\boldsymbol{n}\left(1+\frac{\boldsymbol{B}\cdot\boldsymbol{n}}{\boldsymbol{v}\cdot\boldsymbol{n}}\right)y,\quad K\equiv\int_{\partial D}-(2H)_\delta\, y. \tag{1.10}$$

The viscous dissipation Φ in (1.10) generally depends on γ, and its nonlinear dependence on γ has been exhibited in the special case of the free viscous drop (Prosperetti 1980*b*).

There is a considerable literature on viscous corrections, in the form of $\exp(-\kappa t)$ with damping coefficients κ, to the inviscid oscillations of droplets. Schematically, (1.9) is evaluated at a solution to the inviscid field equations using some approximation of the dependence of Φ on γ. The oldest approximation goes back to Lamb (1932) who evaluated Φ in (1.10) using irrotational motions $\boldsymbol{B}=0$ to find

$$\kappa=\frac{\nu}{R^2}(n-1)(2n+1), \tag{1.11}$$

where ν is the kinematic viscosity. Alternative approximation schemes are still being introduced. Joseph and coworkers (Padrino, Funada & Joseph 2007) have given them names such as 'viscous potential flow' and the 'dissipation method'. These approximation schemes could also be applied to the spherical-belt solutions we report.

Most relevant to the problem considered here are papers invoking spherical-like constraints. Strani & Sabetta (1984, 1988) consider the linear oscillations of both inviscid and viscous drops in partial contact with a 'spherical bowl' by using a Green's function approach to derive an integral eigenvalue equation, which is then reduced to a set of linear algebraic equations by a Legendre series expansion. They report a new low-frequency mode, not present for isolated drops, and exponential eigenfrequency growth as the size of the spherical bowl is increased from a point to a fully captured sphere. Strani & Sabetta (1988) require their viscous drop to satisfy the shear boundary conditions by a means that differs from ours, but their governing equation could also be placed in the context of the operator formalism used here. For small support angles, Strani & Sabetta's results compare well with experiments on supported immiscible drops (Rodot, Bisch & Lasek 1979; Bisch, Lasek & Rodot 1982) and supported drops in microgravity (Rodot & Bisch 1984). Bauer & Chiba (2004, 2005) have also investigated spherical 'bowl-like' constraints for inviscid and viscous captured drops by approximating finite-sized constraints with a large number of point-wise constraints.

We begin this paper by defining the linearized field equations and relevant boundary conditions for the viscous problem, from which the equation of motion for the drop interface is derived and formulated as an eigenvalue problem on linear operators. The operator eigenvalue equation is reduced to a truncated set of linear algebraic equations using a spectral method on a constrained function space, as described in Part 1. The eigenvalues/modes are then computed from a nonlinear characteristic equation, which depends upon material properties and the size/location of the constraint. We conclude with some remarks on the computational results.

2. Mathematical formulation

Consider an unperturbed spherical droplet of radius R, constrained by a spherical belt over the polar angle $\theta_2 \leqslant \theta \leqslant \theta_1$ in spherical coordinates (r, θ), as shown in the definition sketch (figure 1). The drop interface is disturbed by time-dependent free-surface perturbations, $\eta_1(\theta, t)$ and $\eta_2(\theta, t)$, which are assumed to be axisymmetric and small. No domain perturbation is needed for linear problems, thus the domain is the combination of the regions internal to and external to the static droplet:

$$D^i \equiv \{(r, \theta) \mid 0 < r \leqslant R, 0 \leqslant \theta \leqslant \pi\}, \tag{2.1a}$$

$$D^e \equiv \{(r, \theta) \mid R < r < \infty, 0 \leqslant \theta \leqslant \pi\}. \tag{2.1b}$$

The interface separating the interior and exterior fluids (internal boundary) is defined as the union of two free surfaces and one surface of support:

$$\partial D_1^f \equiv \{(r, \theta) \mid r = R, \theta_1 \leqslant \theta \leqslant \pi\}, \tag{2.2a}$$

$$\partial D_2^f \equiv \{(r, \theta) \mid r = R, 0 \leqslant \theta \leqslant \theta_2\}, \tag{2.2b}$$

$$\partial D^s \equiv \{(r, \theta) \mid r = R, \theta_2 \leqslant \theta \leqslant \theta_1\}, \tag{2.2c}$$

$$\partial D \equiv \partial D_1^f \cup \partial D_2^f \cup \partial D^s. \tag{2.2d}$$

The inner and exterior fluids are viscous and incompressible and the effect of gravity is neglected.

2.1. *Field equations*

The field equations, governing the motion of the fluid, are written via a velocity field $\boldsymbol{u}$ and pressure P. An incompressible fluid necessarily has a divergence-free velocity field,

$$\nabla \cdot \boldsymbol{u} = 0. \tag{2.3}$$

The linear momentum balance on a material volume gives the linearized Navier–Stokes equation

$$\rho \frac{\partial \boldsymbol{u}}{\partial t} = -\nabla P - \mu \nabla \times \nabla \times \boldsymbol{u}, \tag{2.4}$$

where the material properties, ρ and μ, are the fluid density and viscosity, respectively. Applying the curl to (2.4) gives the balance of angular momentum

$$\rho \frac{\partial \boldsymbol{\Omega}}{\partial t} = -\mu \nabla \times \nabla \times \boldsymbol{\Omega}, \tag{2.5}$$

with the vorticity $\boldsymbol{\Omega}$ defined as

$$\boldsymbol{\Omega} \equiv \nabla \times \boldsymbol{u}. \tag{2.6}$$

2.2. *Velocity field*

The velocity field for axisymmetric flows is written in spherical coordinates as

$$\boldsymbol{u} = u_r(r, \theta, t)\, \boldsymbol{e}_r + u_\theta(r, \theta, t)\, \boldsymbol{e}_\theta. \tag{2.7}$$

Here we have assumed a flow without swirl $u_\phi(r, \theta, t)$, although swirl can be easily added (see appendix C). According to the velocity field (2.7), the vorticity is

$$\boldsymbol{\Omega} = \Omega(r, \theta, t)\, \boldsymbol{e}_\phi = \frac{1}{r}\left[u_\theta + r\frac{\partial u_\theta}{\partial r} - \frac{\partial u_r}{\partial \theta}\right] \boldsymbol{e}_\phi. \tag{2.8}$$

2.3. *Reduced system*

Substitution of normal modes

$$u_r\,(r,\theta,t)=v_r\,(r,\theta)\,\mathrm{e}^{-\gamma t},\quad u_\theta\,(r,\theta,t)=v_\theta\,(r,\theta)\,\mathrm{e}^{-\gamma t},\tag{2.9a}$$

$$\Omega\,(r,\theta,t)=\omega\,(r,\theta)\,\mathrm{e}^{-\gamma t},\quad P\,(r,\theta,t)=p\,(r,\theta)\,\mathrm{e}^{-\gamma t},\tag{2.9b}$$

$$\eta_{1,2}(\theta,t)=y_{1,2}\,(\theta)\,\mathrm{e}^{-\gamma t},\tag{2.9c}$$

into the hydrodynamic equations (2.3)–(2.6) delivers a reduced set of field equations,

$$\nabla\cdot\boldsymbol{v}=0,\tag{2.10a}$$

$$\rho\gamma\boldsymbol{v}=\nabla p+\mu\nabla\times\nabla\times\boldsymbol{v},\tag{2.10b}$$

$$\rho\gamma\boldsymbol{\omega}=\mu\nabla\times\nabla\times\boldsymbol{\omega},\tag{2.10c}$$

$$\boldsymbol{\omega}=\nabla\times\boldsymbol{v},\tag{2.10d}$$

valid in both interior (i) and exterior (e) sub-domains. Here γ is the complex growth rate.

2.4. *Boundary/integral conditions*

The no-slip and no-penetration conditions for viscous fluids require

$$v_\theta^{i,e}=0\,[\partial D^s],\tag{2.11a}$$

$$v_r^{i,e}=0\,[\partial D^s],\tag{2.11b}$$

on the surface of support, while continuity of tangential velocity and shear stress

$$v_\theta^i=v_\theta^e\left[\partial D_1^f,\partial D_2^f\right],\tag{2.12a}$$

$$\tau_{r\theta}^i=\tau_{r\theta}^e\left[\partial D_1^f,\partial D_2^f\right],\tag{2.12b}$$

is enforced on the free surfaces. The linearized kinematic condition relates the radial velocity to the surface deformation there,

$$v_r^i=v_r^e=-\gamma y_{1,2}(\theta)\left[\partial D_1^f,\partial D_2^f\right],\tag{2.13}$$

and the difference in normal stress across the free surface is balanced by the surface tension σ times the linearized curvature of the deformed surface,

$$\tau_{rr}^i-\tau_{rr}^e=-\frac{\sigma}{R^2}\left(\frac{1}{\sin\theta}\frac{\partial}{\partial\theta}\left(\sin\theta\,\frac{\partial y_{1,2}}{\partial\theta}\right)+2y_{1,2}\right)\left[\partial D_1^f,\partial D_2^f\right].\tag{2.14}$$

The integral form of the incompressibility condition (2.3) constrains the interface perturbation to be volume conserving,

$$\int_{\theta_1}^{\pi}y_1(\theta,t)\sin\theta\,\mathrm{d}\theta+\int_0^{\theta_2}y_2(\theta,t)\sin\theta\,\mathrm{d}\theta=0.\tag{2.15}$$

The fluids are assumed to be Newtonian, where the components of stress are related to the velocity-field components. In spherical coordinates, these relationships are

$$\tau_{r\theta}=\tau_{\theta r}=\mu\left(\frac{1}{r}\frac{\partial v_r}{\partial\theta}+\frac{\partial v_\theta}{\partial r}-\frac{v_\theta}{r}\right),\tag{2.16a}$$

$$\tau_{rr}=-p+2\mu\frac{\partial v_r}{\partial r}.\tag{2.16b}$$

2.5. *Velocity-field decomposition*

The Helmholtz decomposition theorem (e.g. Batchelor 1967) allows one to decompose the velocity field as the sum of rotational and irrotational fields. The vorticity field $\boldsymbol{\omega}$ is solenoidal and therefore may be written as the curl of a vector potential $\boldsymbol{B}$,

$$\boldsymbol{\omega} = \nabla \times \boldsymbol{B}, \tag{2.17}$$

where for axisymmetric flows with non-trivial interface deflection (Chandrasekhar 1961),

$$\boldsymbol{B} = B\,(r,\theta)\,\boldsymbol{e}_r. \tag{2.18}$$

Given (2.17), the velocity field $\boldsymbol{v}$ is decomposed as

$$\boldsymbol{v} = \boldsymbol{B} + \nabla\Psi, \tag{2.19}$$

with the scalar field Ψ defined as the velocity potential. Let $x \equiv \cos(\theta)$, then the velocity-field components are

$$\boldsymbol{v} = \left(B + \frac{\partial\Psi}{\partial r}\right)\boldsymbol{e}_r - \left(\frac{1}{r}\left(1-x^2\right)^{1/2}\frac{\partial\Psi}{\partial x}\right)\boldsymbol{e}_\theta. \tag{2.20}$$

Similar to the field quantities, the vector and velocity potentials are expanded with normal modes

$$B\,(r,x,t) = T_n\,(r)\,P_n\,(x)\,\mathrm{e}^{-\gamma t}, \quad \Psi\,(r,x,t) = \phi_n\,(r)\,P_n\,(x)\,\mathrm{e}^{-\gamma t}, \tag{2.21}$$

where $P_n(x)$ is the Legendre polynomial of degree n.

2.6. *Velocity-field equations*

The rotational field (2.18) satisfies the vorticity equation (2.10*c*). Substituting the normal mode (2.21) into (2.10*c*) generates an equation governing $T_n(r)$,

$$\frac{\mu}{\rho}\frac{\mathrm{d}^2T_n}{\mathrm{d}r^2} + \gamma T_n - \frac{\mu}{\rho}\frac{n\,(n+1)}{r^2}T_n = 0. \tag{2.22}$$

The velocity potential ϕ is chosen such that the incompressibility condition (2.10*a*) is satisfied. Substituting (2.20) and (2.21) into (2.10*a*) results in an inhomogeneous equation for $\phi_n(r)$,

$$\nabla^2\left(\phi_n\,(r)\,P_n\,(x)\right) = -\frac{1}{r^2}\frac{\mathrm{d}}{\mathrm{d}r}\left(r^2T_n\right)P_n\,(x)\,. \tag{2.23}$$

A general solution for the velocity field (2.19) is constructed by solving (2.22) and (2.23).

3. Reduction to an operator equation

Equations (2.10)–(2.15) constitute an eigenvalue problem for the complex growth rate γ. In this section, the boundary-value problem is reduced to a single integro-differential equation, which is then formulated as an eigenvalue equation on linear operators. To that end, the goal is to construct solutions to the field (2.10)–(2.15) for this capillary-driven flow that depend explicitly upon the free-surface deformations y_1, y_2. As in Part 1, we begin by defining the 'interface' perturbation as

$$y(x) = \begin{cases} y_1(x), & -1 \leqslant x \leqslant \zeta_1, \\ 0, & \zeta_1 \leqslant x \leqslant \zeta_2, \\ y_2(x), & \zeta_2 \leqslant x \leqslant 1. \end{cases} \tag{3.1}$$

Here the parameters

$$\zeta_1 \equiv \cos(\theta_1), \quad \zeta_2 \equiv \cos(\theta_2), \tag{3.2}$$

define the geometry of the spherical-belt constraint. In view of the linearized kinematic condition (e.g. (2.13)) enforced everywhere, the no-penetration condition (2.11*b*) is satisfied by construction for disturbances of the form (3.1). At this point the free-surface deformations y_1, y_2 remain independent. However, the 'shear' boundary conditions (2.11*a*), (2.12*a*) and (2.12*b*) must change from no-stress (free) to no-slip (supported). To address this issue, a modified set of boundary conditions is proposed. A normal-mode analysis with the modified boundary conditions allows one to derive the viscous operator equation, which depends upon a viscosity parameter ϵ, the ratio of inner to exterior densities ρ, the ratio of inner to exterior viscosities μ, and a support size parameter.

3.1. *Vector potential solution*

The vector potential solution of (2.22) is given by

$$T_n^i(r) = \left(\frac{r}{R}\right)^{1/2} T_n^i(R) \frac{\mathrm{J}_{n+1/2}\left(z^i\right)}{\mathrm{J}_{n+1/2}\left(Z^i\right)}, \quad T_n^e(r) = \left(\frac{r}{R}\right)^{1/2} T_n^e(R) \frac{\mathrm{H}_{n+1/2}^{(1)}\left(z^e\right)}{\mathrm{H}_{n+1/2}^{(1)}\left(Z^e\right)}, \tag{3.3}$$

where

$$z^{i,e} \equiv r\left(\gamma \frac{\rho_{i,e}}{\mu_{i,e}}\right)^{1/2}, \quad Z^{i,e} \equiv R\left(\gamma \frac{\rho_{i,e}}{\mu_{i,e}}\right)^{1/2}, \tag{3.4}$$

and $\mathrm{J}_k(z)$ and $\mathrm{H}_k^{(1)}(z)$ are the appropriate Bessel functions (standard notation used, Arfken & Weber 2001).

3.2. *Velocity potential solution*

Equation (2.23) is solved using variation of parameters for the velocity potential,

$$\begin{aligned} \phi_n^{i,e}(r) = {} & \left(\alpha_n^{i,e} - \frac{n+1}{2n+1} \int_R^r \frac{T_n^{i,e}(s)}{s^n}\, \mathrm{d}s\right) r^n \\ & + \left(\beta_n^{i,e} - \frac{n}{2n+1} \int_R^r s^{n+1} T_n^{i,e}(s)\, \mathrm{d}s\right) r^{-(n+1)}. \end{aligned} \tag{3.5}$$

The velocity potential is finite as $r \to 0$ and $r \to \infty$, which requires

$$\beta_n^i = -\frac{n}{2n+1} \int_0^R s^{n+1} T_n^i(s)\, \mathrm{d}s = -\frac{n}{2n+1} \frac{T_n^i(R)}{\mathrm{J}_{n+3/2}\left(Z^i\right)} R^{n+2} \tag{3.6}$$

and

$$\alpha_n^e = \frac{n+1}{2n+1} \int_R^\infty \frac{T_n^e(s)}{s^n}\, \mathrm{d}s = \frac{n+1}{2n+1} \frac{T_n^e(R)}{\mathrm{H}_{n-1/2}\left(Z^e\right)} R^{-(n-1)}, \tag{3.7}$$

where

$$\mathrm{J}_k(z) \equiv z \frac{\mathrm{J}_{k-1}(z)}{\mathrm{J}_k(z)}, \quad \mathrm{H}_k(z) \equiv z \frac{\mathrm{H}_{k+1}^{(1)}(z)}{\mathrm{H}_k^{(1)}(z)} \tag{3.8}$$

are fractional Bessel functions (again standard notation, Arfken & Weber 2001).

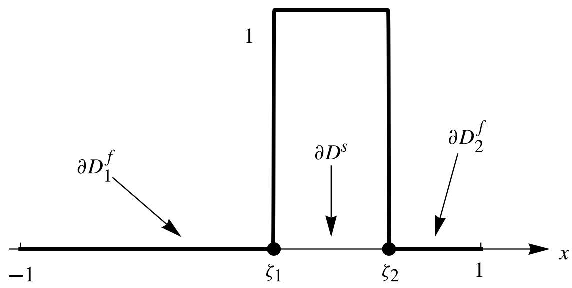

FIGURE 2. Indicator function $\Gamma(x, \zeta_1, \zeta_2)$.

3.3. *Boundary conditions*

As with the other field quantities, the interface perturbation is expanded as

$$y(x) = \sum_{n=1}^{\infty} d_n P_n(x), \quad d_n \equiv \frac{(y, P_n)}{(P_n, P_n)}. \tag{3.9}$$

Using (2.20) and (3.9), the linearized kinematic condition (2.13) is reduced to

$$T_n^i(R) + \left.\frac{\mathrm{d}\phi_n^i}{\mathrm{d}r}\right|_{r=R} = -\gamma d_n, \quad T_n^e(R) + \left.\frac{\mathrm{d}\phi_n^e}{\mathrm{d}r}\right|_{r=R} = -\gamma d_n. \tag{3.10}$$

As in Part 1, (3.10) is enforced on the entire interface, and the no-penetration condition (2.11*b*) is satisfied by restricting candidate functions to an appropriately chosen function space. To simplify (3.10), use the velocity potential solution (3.5) to obtain

$$\alpha_n^i = \frac{n+1}{n} R^{-(2n+1)} \beta_n^i - \frac{\gamma}{n} R^{-(n-1)} d_n, \quad \beta_n^e = \frac{n}{n+1} R^{2n+1} \alpha_n^e + \frac{\gamma}{n+1} R^{n+2} d_n, \tag{3.11}$$

with β_n^i and α_n^e given by (3.6) and (3.7), respectively.

The remaining unknowns, $T_n^i(R)$ and $T_n^e(R)$, are found from the shear boundary conditions: (2.11*a*), (2.12*a*) and (2.12*b*). These boundary conditions are valid on specified parts of the interface and are not amenable to standard analysis. To resolve this issue, a new set of boundary conditions is proposed. On the drop interface, the following equivalent boundary conditions are introduced to replace (2.11*a*), (2.12*a*) and (2.12*b*):

$$v_\theta^i|_{r=R} = v_\theta^e|_{r=R}, \tag{3.12a}$$

$$\left(\tau_{r\theta}^i - \tau_{r\theta}^e\right)|_{r=R} \left(1 - \Gamma(x, \zeta_1, \zeta_2)\right) = (\mu/R)\, \Gamma(x, \zeta_1, \zeta_2)\, v_\theta^i|_{r=R}, \tag{3.12b}$$

with R the length scale and μ the appropriate viscosity scale: μ_i for an immiscible drop in vacuum or viscous medium and μ_e for a bubble in viscous medium. Here $\Gamma(x, \zeta_1, \zeta_2)$ is an indicator function, which is active on the surface of support and inactive on the free surfaces (cf. figure 2),

$$\Gamma(x, \zeta_1, \zeta_2) \equiv H(x - \zeta_1) - H(x - \zeta_2), \tag{3.13}$$

where $H(x)$ is the Heaviside step function.

3.4. *Pressure*

The pressure is found by substituting (2.21) into (2.10*b*) to give

$$p(r,x)=p_0+\sum_{n=1}^{\infty}\rho\left(\gamma\phi_n-\frac{\mu}{\rho}\frac{\mathrm{d}T_n}{\mathrm{d}r}\right)P_n(x). \tag{3.14}$$

Using the vector and velocity potential solutions (3.3) and (3.5), the pressure evaluated on the surface is

$$p^i(R,x)=p_0^i-\sum_{n=1}^{\infty}\left((n+1)\,\mu_i\frac{T_n^i(R)}{R}+\frac{\rho_i R\gamma^2}{n}d_n\right)P_n(x), \tag{3.15a}$$

$$p^e(R,x)=p_0^e+\sum_{n=1}^{\infty}\left(n\,\mu_e\frac{T_n^e(R)}{R}+\frac{\rho_e R\gamma^2}{n+1}d_n\right)P_n(x). \tag{3.15b}$$

3.5. *Operator equation*

The operator equation is derived from the normal-stress boundary condition (2.14),

$$-p^i+2\mu_i\left.\frac{\partial v_r^i}{\partial r}\right|_{r=R}+p^e-2\mu_e\left.\frac{\partial v_r^e}{\partial r}\right|_{r=R}=-\frac{\sigma}{R^2}\left(\left(1-x^2\right)y_{xx}-2xy_x+2y\right), \tag{3.16}$$

which can be written as

$$\begin{aligned}\sum_{n=1}^{\infty}\Bigg[&\left(\left(\frac{\rho_e}{n+1}+\frac{\rho_i}{n}\right)\gamma^2R+2\,(n-1)\,(n+2)\,(\mu_i-\mu_e)\,\frac{\gamma}{R}\right)d_n\\&+n\,(n+2)\,\mu_e\frac{T_n^e(R)}{R}-(n-1)\,(n+1)\,\mu_i\frac{T_n^i(R)}{R}\Bigg]P_n(x)\\&=-\frac{\sigma}{R^2}\left(\left(1-x^2\right)y_{xx}-2xy_x+2y\right),\end{aligned} \tag{3.17}$$

with $T_n^i(R)$ and $T_n^e(R)$ determined from the modified boundary conditions (3.12). This is done in appendix A.

We now scale the interface deformation y, $y\equiv Ry^*$, drop the * for notational simplicity henceforth, and introduce the further scalings

$$\gamma^*\equiv\sqrt{\frac{\rho_iR^3}{\sigma}}\gamma,\quad \epsilon_{i,e}\equiv\frac{\mu_{i,e}}{\sqrt{\rho_{i,e}R\sigma}},\quad \mu\equiv\frac{\mu_e}{\mu_i},\quad \rho\equiv\frac{\rho_e}{\rho_i}. \tag{3.18}$$

A characteristic of the modified boundary conditions is a 'shape' factor

$$L_n=\left(\int_{-1}^{1}\left(P_n^{(1)}(x)\right)^2\Gamma(x,\zeta_1,\zeta_2)\,\mathrm{d}x\right)\left(\frac{2n+1}{2}\frac{(n-1)!}{(n+1)!}\right), \tag{3.19}$$

which is a measure of the relative size of the surface of support. Here $P_n^{(1)}(x)$ is the Legendre polynomial of degree n and order one (MacRobert 1967).

3.5.1. *Drop in vacuum*

A viscous drop in a vacuum corresponds to the limiting case $\mu_e\to0$ and $\rho_e\to0$. In this limit, the viscous drop operator equation is given by

$$\gamma^{*2}M_d[y]+\gamma^*\Phi_d\left[y;\gamma^*,\epsilon_i\right]+K[y]=0. \tag{3.20}$$

The differential operator

$$K[y] \equiv \left(1 - x^2\right) y_{xx} - 2xy_x + 2y \tag{3.21}$$

is associated with the curvature, while the positive-definite inertia operator is defined as

$$M_d[y] \equiv \sum_{n=1}^{\infty} \frac{1}{n} \left(\frac{2n+1}{2}\right) \left(\int_{-1}^{1} y P_n \mathrm{d}x\right) P_n(x). \tag{3.22}$$

Viscous effects are controlled by the dissipation operator

$$\begin{aligned} \Phi_d\left[y; \gamma^*, \epsilon_i\right] \equiv -\epsilon_i \sum_{n=1}^{\infty} &\left[\left(2(n-1)(n+2) + (n-1)(n+1) T_n^i(R)\right)\right. \\ &\times \left.\left(\frac{2n+1}{2}\right) \left(\int_{-1}^{1} y P_n \mathrm{d}x\right) P_n(x)\right], \end{aligned} \tag{3.23}$$

where

$$T_n^i(R) = \frac{2(n-1)/n - \epsilon_i A_n/n}{\left(2/\mathrm{J}_{n+3/2}(X^i) - 1\right) + \epsilon_i A_n/\mathrm{J}_{n+3/2}(X^i)} \tag{3.24}$$

and

$$A_n \equiv L_n/(1 - L_n), \quad X^i \equiv (\gamma^*/\epsilon_i)^{1/2}. \tag{3.25}$$

3.5.2. *Bubble in viscous medium*

A similar operator equation is derived for a bubble; the limit $\mu_i \to 0$ and $\rho_i \to 0$ of (3.17) gives

$$\gamma^{*2} M_b[y] + \gamma^* \Phi_b\left[y; \gamma^*, \epsilon_e\right] + K[y] = 0, \tag{3.26}$$

where the curvature operator is defined in (3.21) and the inertia operator for a bubble as

$$M_b[y] \equiv \sum_{n=1}^{\infty} \frac{1}{n+1} \left(\frac{2n+1}{2}\right) \left(\int_{-1}^{1} y P_n \mathrm{d}x\right) P_n(x). \tag{3.27}$$

The bubble dissipation operator is given by

$$\begin{aligned} \Phi_b\left[y; \gamma^*, \epsilon_e\right] \equiv -\epsilon_e \sum_{n=1}^{\infty} &\left[\left(-2(n-1)(n+2) + n(n+2) T_n^e(R)\right)\right. \\ &\times \left.\left(\frac{2n+1}{2}\right) \left(\int_{-1}^{1} y P_n \mathrm{d}x\right) P_n(x)\right], \end{aligned} \tag{3.28}$$

with

$$T_n^e(R) = -\frac{2(n+2)/(n+1) - \epsilon_e A_n/(n+1)}{\left(2/\mathrm{H}_{n-1/2}(X^e) - 1\right) + \epsilon_e A_n/\mathrm{H}_{n-1/2}(X^e)} \tag{3.29}$$

and

$$A_n \equiv L_n/(1 - L_n), \quad X^e \equiv (\gamma^*/\epsilon_e)^{1/2}. \tag{3.30}$$

3.5.3. *Immiscible viscous drop in viscous medium*

The operator equation for the case of an immiscible viscous drop in a viscous medium is the most general case. This operator equation is displayed in appendix B.

4. Solution of the operator equation

The operator equation (3.20), (3.26) and (B 1) are nonlinear in the eigenvalue and can be reduced to a set of algebraic equations using a spectral approach with the function space derived in Part 1. We shall present results for the viscous drop in a vacuum (3.20) and the bubble in a viscous bath (3.26). The resulting matrix equation is parameterized by the viscosity parameter ϵ (representing ϵ_i or ϵ_e) and the boundaries of the constraint, ζ_1 and ζ_2, via the indicator function $\varGamma(x, \zeta_1, \zeta_2)$. The eigenvalues/eigenmodes are then computed from a nonlinear characteristic equation, found by taking the determinant of the matrix equation.

4.1. *Constrained function space*

To implement the spectral method on the operator equation (3.20) and (3.26), one needs to construct a function space for the interface perturbation (3.1) that satisfies the following conditions:

$$\int_{-1}^{\zeta_1} y_1(x)\,\mathrm{d}x + \int_{\zeta_2}^{1} y_2(x)\,\mathrm{d}x = 0, \tag{4.1a}$$

$$y_1(\zeta_1) = 0, \tag{4.1b}$$

$$y_2(\zeta_2) = 0. \tag{4.1c}$$

Equation (4.1*a*) is the incompressibility condition that couples the independent free-surface perturbations, y_1 and y_2, while (4.1*b*) and (4.1*c*) ensure the interface perturbation (3.1) is single-valued. Once again, recall that the no-penetration condition is satisfied by the form of (3.1). For brevity, we refer the reader to Part 1 for details regarding the construction of a set of orthonormal basis functions $\{\psi_k\}$ that span the constrained function space and satisfy (4.1). A similar method has been used in the context of constrained cylindrical interfaces by Bostwick & Steen (2010).

4.2. *Reduction to matrix form*

A truncated series expansion

$$y(x) = \sum_{k=1}^{N} c_k \psi_k(x), \tag{4.2}$$

is applied to the operator equations (3.20) and (3.26) and inner products are taken to yield the following set of algebraic equations for c_k:

$$\sum_{k=1}^{N} \left(\gamma^{*2} M_{jk} + \gamma^{*} \varPhi_{jk}(\gamma^{*}, \epsilon) + K_{jk}\right) c_k = 0_j, \tag{4.3}$$

with

$$M_{jk} \equiv \int_{-1}^{1} M[\psi_j]\psi_k\,\mathrm{d}x, \quad \varPhi_{jk} \equiv \int_{-1}^{1} \varPhi[\psi_j]\psi_k\,\mathrm{d}x, \quad K_{jk} \equiv \int_{-1}^{1} K[\psi_j]\psi_k\,\mathrm{d}x. \tag{4.4}$$

The solvability condition for the matrix equation (4.3) is a zero determinant, which results in a nonlinear characteristic equation. The roots of the characteristic equation generate the complex eigenvalue $\gamma^{*(p)}$ and eigenvector $c_j^{(p)}$, while the corresponding eigenfunction is given by

$$y^{(p)}(x) = \sum_{k=1}^{N} c_k^{(p)} \psi_k(x). \tag{4.5}$$

5. Validation of the solution

The eigenvalues/modes for the drop and bubble, as they depend upon the viscosity parameter ϵ, are the roots of a nonlinear characteristic equation and are computed using a variant of the secant method. We generate initial guesses for the secant method by continuation of the inviscid solution (Part 1) in the viscosity parameter. The characteristic equation is computed using $N = 13$ terms in the solution series (4.2), with a resolution of eight Legendre polynomials on each free surface. This truncation is shown to produce relative eigenvalue convergence to within 0.1 % for the results presented here, except near critical damping, the transition between complex and real eigenvalues. The complex eigenvalues presented here appear in complex-conjugate pairs.

A number of limiting cases are evaluated next to verify both the numerical routine as well as the modified boundary conditions (3.12). The inviscid limit $\mu_i \to 0$, $\mu_e \to 0$ of (3.17) recovers operator equation (3.7) of Part 1 and, hence, all the inviscid results of Part 1 are special-case solutions of (3.17). Our focus next is on special viscous solutions.

5.1. *Pinned circle-of-contact limits*

Just as for the inviscid drop, pinning at a circle of contact $(\zeta_1, \zeta_2) = \zeta(1, 1)$ which is also a node ζ of the eigenmode, recovers the unconstrained drop behaviour. In the viscous case, we locate the constraint at the node of a Legendre polynomial and compare to the free viscous drop solution of (Prosperetti 1980*b*). In this limit, the 'shape' factor (3.19) tends to zero and the operator equations (3.20) and (3.26) can be manipulated into the functional equivalent of the Prosperetti (1980*b*) equations for the free drop. As shown in Part 1, the no-penetration condition (2.11*b*) is naturally satisfied for this specific constraint and the corresponding frequency and mode shape are identical to those for the free viscous drop (Prosperetti 1980*b*).

5.2. *Spherical-bowl limits*

The limit $\zeta_1 \to -1$ ($\theta_1 = 180°$) of a spherical belt yields a spherical-bowl support of extent $\zeta_2 = \zeta$ analysed by Strani & Sabetta (1988). 'Small bowl' ('large bowl') will refer to a support less than (greater than) hemispherical in extent, likewise for belt supports.

For a bubble in a viscous bath supported by a small bowl of extent $\zeta = -0.5$ ($\theta = 120°$), there are no transitions from under-damped to over-damped motions according to figure 3. The bubble motions remain under-damped. For a fixed mode, the damping rate increases with ϵ_e as the viscous layer penetrates deeper into the bath until the frequency rapidly decreases to pull the damping rate back down. This may be viewed as a partitioning of dissipation between spatial and temporal contributions. For fixed ϵ_e, higher modes have higher damping consistent with the greater dissipation at smaller length scales. Figure 3 can be compared to Strani & Sabetta (1988), figure 2, and the agreement is excellent (truncation numbers N are comparable).

In contrast, for a viscous drop in a vacuum supported by a small bowl, $\zeta = -0.94$ ($\theta = 160°$), there is a transition from under- to over-damped, figure 4. The $n = 1, 2, 3$

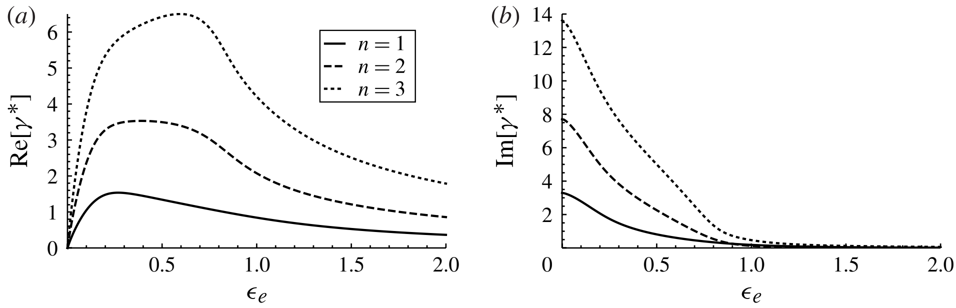

FIGURE 3. Bubble with small-bowl support $\zeta = -0.5$ ($\theta = 120°$): (*a*) decay rate Re[γ^*] and (*b*) oscillation frequency Im[γ^*] against viscosity parameter ϵ_e for modes $n = 1, 2, 3$.

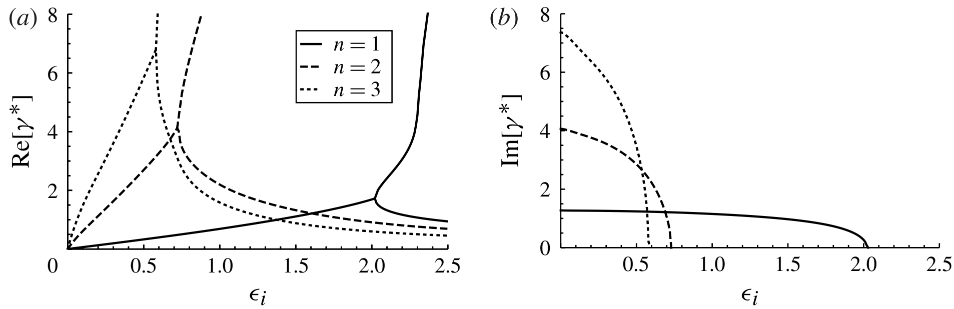

FIGURE 4. Viscous drop with small-bowl support $\zeta = -0.94$ ($\theta = 160°$): (*a*) decay rate Re[γ^*] and (*b*) oscillation frequency Im[γ^*] against viscosity parameter ϵ_i for modes $n = 1, 2, 3$.

eigenvalues bifurcate from complex to real at a critical value of the viscosity parameter. This critical value is smaller for the $n = 3$ mode compared with the $n = 2$ mode because there is stronger relative motion between fluid elements for $n = 3$. Figure 4 can be compared to Strani & Sabetta (1988), figure 3, and the agreement is excellent (truncation numbers N are comparable).

The eigenvalues in these plots are obtained by finding the zeros of a nonlinear equation given by the determinant of (4.3). As the truncation number N increases, so do the number of roots. Strani & Sabetta (1988) found that the transition from complex to real roots was especially sensitive to N and, for that reason, that the prediction of the transition from under-damped to over-damped motion was not reliable. For further details, the reader is referred to the lengthy discussion provided by Strani & Sabetta (1988). Our spherical-belt calculations face the same difficulty. As a consequence, results near the transition point have large uncertainty.

6. Spherical-belt results

The bubble and drop with small-belt support $(\zeta_1, \zeta_2) = (-0.7, 0)$ $[(\theta_1, \theta_2) = (134°, 90°)]$ have the frequencies reported in figures 5 and 6, respectively. The dissipation arising from relative fluid motion is very apparent when one compares the decay rate of the $n = 1$ mode to the $n = 2, 3$ modes, where the magnitude is much more pronounced for the higher mode numbers. The belt geometry is the same as that

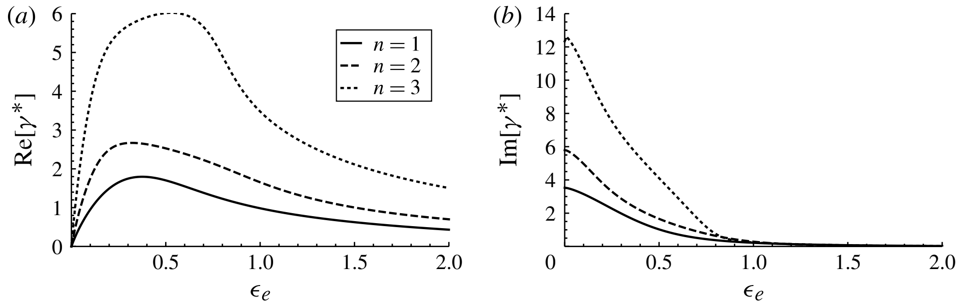

FIGURE 5. Bubble in viscous bath with belt support $(\zeta_1, \zeta_2) = (-0.7, 0.0)$ $[(\theta_1, \theta_2) = (134^\circ, 90^\circ)]$: (*a*) decay rate $\mathrm{Re}[\gamma^*]$ and (*b*) oscillation frequency $\mathrm{Im}[\gamma^*]$ against viscosity parameter ϵ_e for modes $n = 1, 2, 3$.

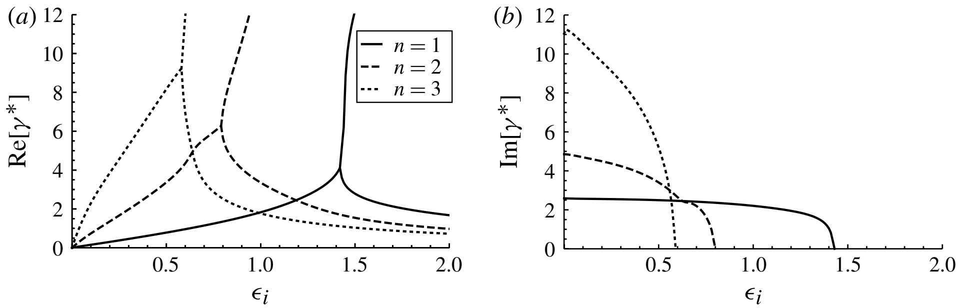

FIGURE 6. Viscous drop with belt support $(\zeta_1, \zeta_2) = (-0.7, 0.0)$ $[(\theta_1, \theta_2) = (134^\circ, 90^\circ)]$: (*a*) decay rate $\mathrm{Re}[\gamma^*]$ and (*b*) oscillation frequency $\mathrm{Im}[\gamma^*]$ against viscosity parameter ϵ_i for modes $n = 1, 2, 3$.

for the inviscid modes, figure 4, Part 1. Even though viscosity has a strong influence on the frequencies, the mode shapes shown in figure 7(*a–c*) cannot be distinguished from those in figure 4(*a–c*), Part 1, at least for $\epsilon \leqslant \epsilon_c$. Later, we shall use this observation to estimate ϵ_c ('frozen interface' approximation).

Figure 7 also plots the streamlines (*d–f*), vector potential (*g–i*) and velocity potential (*j–l*) associated with modes $n = 1$ (*a,d,g,j*), $n = 2$ (*b,e,h,k*) and $n = 3$ (*c,f,i,l*). A comparison between the flow field (*d–f*) for viscous motions to that for inviscid motions (cf. figure 4 (*d–f*), Part 1) shows that the viscous motion is more complex, particularly near the solid support. Specifically, figure 7(*f*) shows that a stagnation point develops near the solid support for the $n = 3$ mode. The primary difference between the inviscid (Part 1) and viscous (Part 2) motions in this problem is the vorticity equation (2.17) of the flow field. For our problem, the vector potential is a measure of the vorticity. Figure 7(*g–i*) shows that the vector potential (vorticity) for the $n = 2, 3$ modes is localized around the drop surface, whereas for the $n = 1$ mode, the vector potential penetrates deeper into the droplet bulk.

Viscous effects resulting from the no-slip boundary might be expected to scale with the extent of no-slip. To test this, we plot eigenvalues γ^* against the scaled arclength of the spherical-belt support $\theta_1 - \theta_2$, for two different geometries each starting from a pinned circle of constraint, one above the equator, $\cos\theta_1 = 0.4$ ($\theta_1 = 66^\circ$), and the

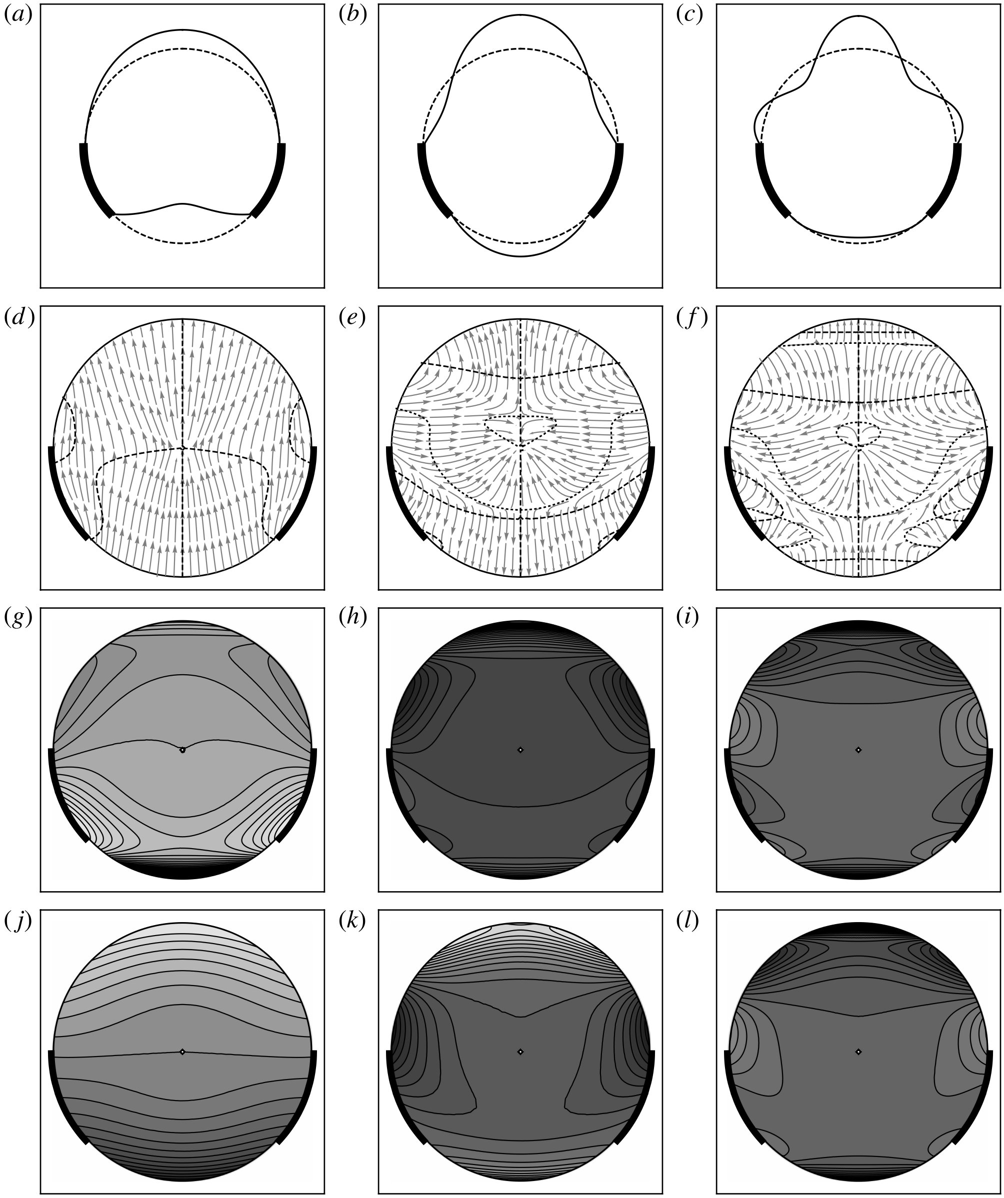

FIGURE 7. Eigenmodes (*a,d,g,j*) $n = 1$, (*b,e,h,k*) $n = 2$, and (*c,f,i,l*) $n = 3$ for viscosity parameter $\epsilon_i = 0.5$, illustrating the (*a–c*) disturbed interface, (*d–f*) streamlines ($\boldsymbol{v}$), (*g–i*) vector potential (B) and (*j–l*) velocity potential (ϕ) for a drop in a vacuum constrained by a spherical belt with $(\zeta_1, \zeta_2) = (-0.7, 0)$ $[(\theta_1, \theta_2) = (134°, 90°)]$. Here the dashed (dotted) curves of (*d–f*) denote points of zero horizontal (vertical) velocity.

other below the equator, $\cos\theta_1 = -0.7$ ($\theta_1 = 134°$), and then widening the circle to a bowl by decreasing θ_2 until $\cos\theta_2 = 1$ ($\theta_2 = 0°$) and to a belt by decreasing θ_2 until $\cos\theta_2 = 0$ ($\theta_2 = 90°$), respectively. In all cases, both decay rate and frequency monotonically increase with $\theta_1 - \theta_2$, consistent with extending the no-slip support and reducing the free surface. On the other hand, the monotonic increase shows

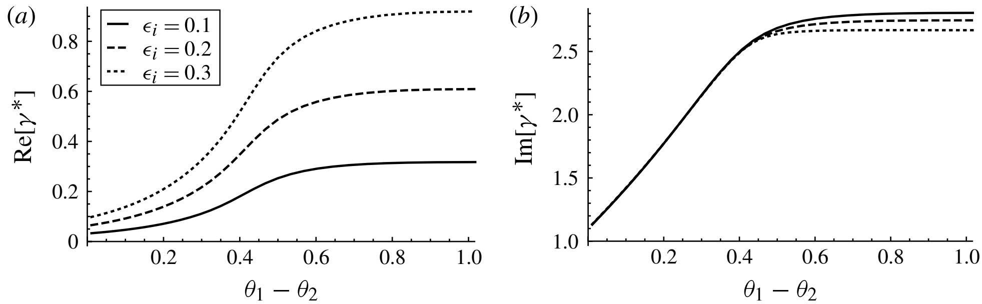

FIGURE 8. For mode number $n = 1$: (*a*) decay rate Re[γ^*] and (*b*) oscillation frequency Im[γ^*] against arclength $\theta_1 - \theta_2$ starting at a pinned circle $\zeta = 0.41$ ($\theta = 66°$, fixed), thickening to a belt and ending at the small-bowl support ($\theta_2 = 0°$) .

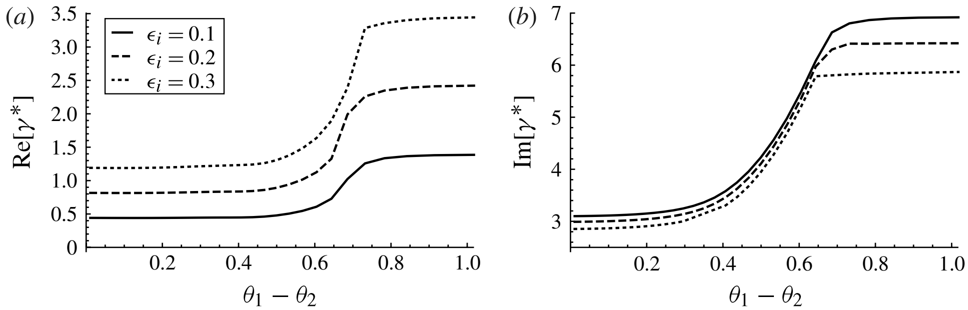

FIGURE 9. For mode number $n = 2$: (*a*) decay rate Re[γ^*] and (*b*) oscillation frequency Im[γ^*] against arclength $\theta_1 - \theta_2$ starting at a pinned circle $\zeta = 0.41$ ($\theta_1 = 66°$, fixed), thickening to a belt and ending at the small-bowl support ($\theta_2 = 0°$).

quite different rates for the different cases. Starting at a pinned circle above the equator, figure 8(*b*) shows that frequency Im[γ^*] increases linearly with belt width and then plateaus. This is consistent with the inviscid behaviour where the frequency increases with extent of support until all the nodes disappear from the free surface. The damping Re[γ^*], figure 8(*a*), in contrast, shows a nonlinear sigmoidal-like growth before plateauing. The growth rate starts below average and then increases to above average. This suggests that both the extent of constraint and the internal structure of the flow contribute. In contrast, for mode $n = 2$, the damping is nearly constant and then abruptly shifts to the plateau, figure 9(*a*), reminiscent of the 'dead' and 'active' regions of the inviscid modes (Part 1). On the other hand, figure 9(*b*), the corresponding frequency increases sub-linearly until it plateaus.

Starting at a pinned circle below the equator for the $n = 1$ mode, the damping and frequency show more gradual transitions to the plateau region, figures 10(*a*) and 10(*b*). For mode $n = 2$, the rates of growth of damping and frequency are similar to those for the mode $n = 2$ above-equator case, except less pronounced, figures 11(*a*) and 11(*b*), respectively. In summary, for both geometries for mode $n = 1$, growths of frequencies are essentially linear with support extent until they plateau, after which the remaining free surface acts much like a rigid support. In contrast, for both geometries

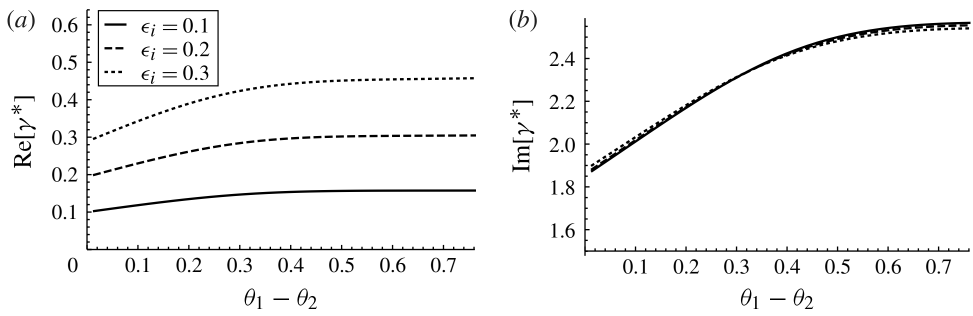

FIGURE 10. For mode number $n = 1$: (*a*) decay rate Re[γ^*] and (*b*) oscillation frequency Im[γ^*] against arclength $\theta_1 - \theta_2$ starting at a pinned circle $\zeta = -0.69$ ($\theta_1 = 134°$, fixed) thickening to a small-belt support $\theta_2 = 90°$.

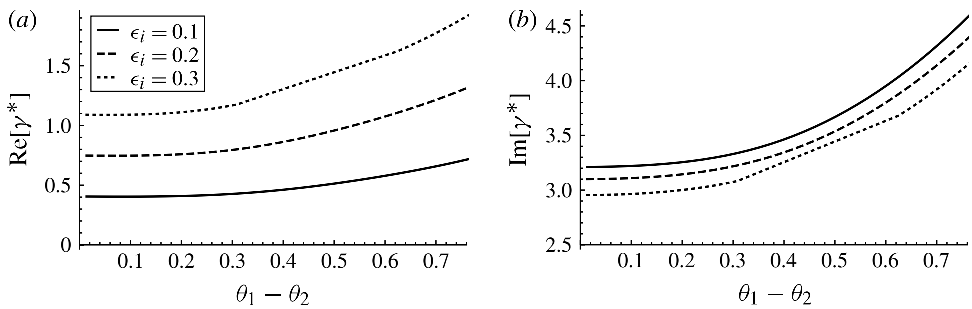

FIGURE 11. For mode number $n = 2$: (*a*) decay rate Re[γ^*] and (*b*) oscillation frequency Im[γ^*] against arclength $\theta_1 - \theta_2$ starting at a pinned circle $\zeta = -0.69$ ($\theta_1 = 134°$, fixed), thickening to a small-belt support $\theta_2 = 90°$.

and both modes, the damping typically increases with support extent in a nonlinear way, suggesting that both the extent of support and internal viscous layers play a role.

6.1. *Critical damping and the 'frozen interface' approximation*

The viscous drop is anticipated to have a critical damping ϵ_c which will depend on location and extent of belt support, important information for applications. Near the critical damping, direct calculation of y_N and γ_N^* with increasing truncation N is not robust, as mentioned above. However, as also noted above, the mode shape for the viscous belted sphere varies little from the inviscid mode shape over a wide range of ϵ_i below ϵ_c. This suggests freezing the interface shape at the inviscid shape in order to find $\gamma^*(\epsilon_i)$ from (1.9) and thereby obtaining $\epsilon_c = \epsilon_c(\zeta_1, \zeta_2)$.

To begin, let y_i^n be the inviscid interface shape of mode number n. Substitute y_i^n into (3.21)–(3.25) to obtain the coefficients of operator equation (3.20). Note that coefficient Φ_d now depends implicitly on unknown γ^*. Taking inner products with y_i^n yields the scalar disturbance energy balance,

$$\gamma^{*2}\left(M_d\left[y_i^n\right], y_i^n\right) + \gamma^*\left(\Phi_d\left[y_i^n; \gamma^*, \epsilon_i\right], y_i^n\right) + \left(K\left[y_i^n\right], y_i^n\right) = 0, \tag{6.1}$$

from which the complex frequency may be computed. Note that the dissipation operator $\Phi_d(\gamma^*)$ includes viscous effects in a way that prior approximations have

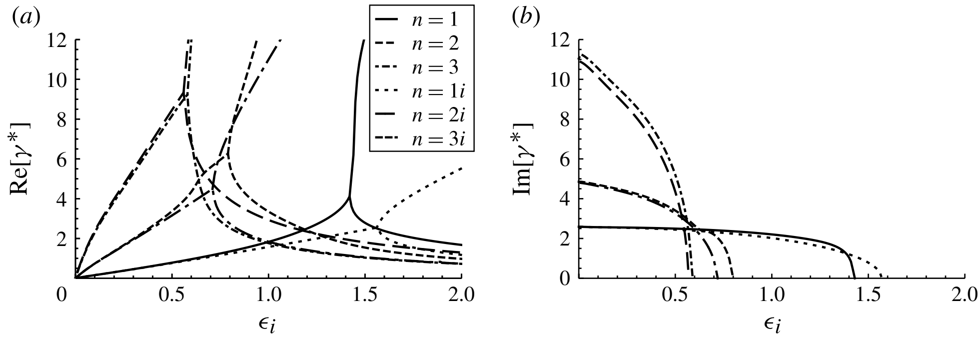

FIGURE 12. Frozen-interface approximation (denoted 'i') for the viscous drop with belt support $(\zeta_1, \zeta_2) = (-0.7, 0)$: (*a*) decay rate Re[$\gamma^*$] and (*b*) oscillation frequency Im[γ^*] against viscosity parameter ϵ_i for modes $n = 1, 2, 3$.

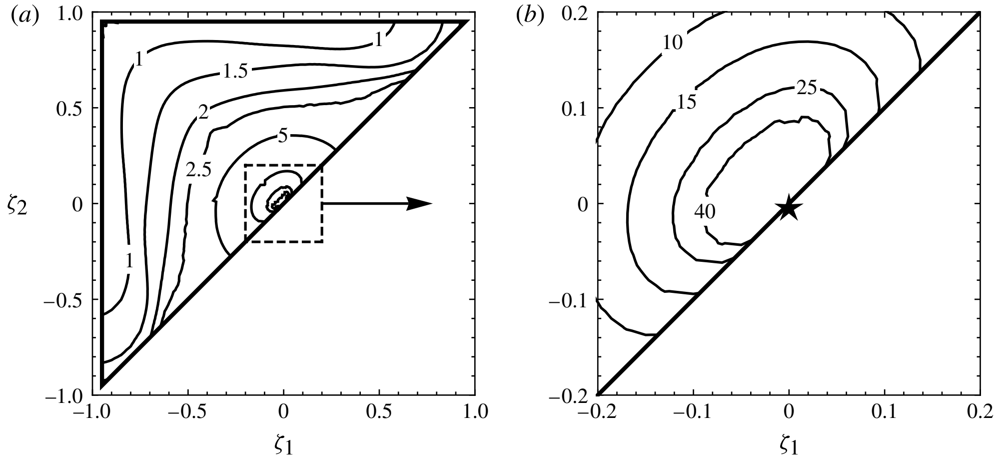

FIGURE 13. Frozen-interface approximation: critical viscosity parameter ϵ_c for the $n = 1$ mode as a function of support size (ζ_1, ζ_2) (*b* is a blow-up of the dashed region in *a*). The limiting case of a pinned circle of contact at the equator $(\zeta_1, \zeta_2) = (0, 0)$ (denoted $\star$ in *b*) recovers the critical viscosity parameter for the free viscous drop $\epsilon_c \to \infty$.

not (cf. the 'viscous potential flow' and 'dissipation method' mentioned in the Introduction).

We find that solutions γ^* of (6.1) for the critical damping parameter ϵ_c converge with increasing truncation number N. Figure 12 plots the solutions of (6.1) as they depend upon the viscosity parameter ϵ_i for the same spherical-belt geometry $(\zeta_1, \zeta_2) = (-0.7, 0)$ and truncation number $N = 13$ used to generate figure 6. Looking at the $n = 1$ mode curves suggests that the relative error for ϵ_c is $\sim$10 %. Note that this is a comparison of two approximations. Figure 13 shows the boundary between under-damped and over-damped motion as it depends on belt size and position, $\epsilon_c = \epsilon_c(\zeta_1, \zeta_2)$. This boundary is important for applications, such as the liquid lens (Olles *et al.* 2011). As shown in figure 13(*b*), the critical viscosity parameter grows very rapidly for small belt sizes in the neighbourhood of the equator. In this region, the mode shapes closely resemble spherical-cap disturbances (see figures 3 and 4*a* in

Part 1), which generate a flow with very little relative motion and small dissipation leading to large values of the critical viscosity parameter. The limiting case of a pinned circle of contact at the equator $\zeta_1 = \zeta_2 = 0$ is a node of the $n = 1$ mode and, as mentioned earlier, recovers the free viscous drop behaviour (Prosperetti 1980*b*). The associated droplet motion consists of a zero-frequency rigid translation with no dissipation and, hence, the critical viscosity parameter $\epsilon_c \to \infty$ (cf. figure 13*b*).

7. Concluding remarks

The linear oscillations of an immiscible, viscous fluid drop, held by surface tension and by a solid support of spherical-belt geometry have been considered here. We have extended the work of Prosperetti (1980*b*) and Strani & Sabetta (1988) to include a latitudinal belt support. Even though the spherical base-state geometry is special, it is likely that our results have a bearing on the behaviour of coupled droplets in similar geometries, much as the coupled spherical-cap model was useful in understanding experimental results for exposed droplets from an overfilled tube (Theisen *et al.* 2007).

The integro-differential equation governing the interface deformation is formulated as an eigenvalue problem on linear operators, of the form of a damped harmonic oscillator. A solution is generated using a spectral method on a constrained function space. The function space is constructed by defining the interface as the union of the three pieces: two free surfaces and one surface of support. Solutions are restricted to these 'allowable' candidate functions. At this level of generality, the free-surface deformations are independent and allowed to communicate, exchanging volume beneath the surface of support while coupled by the overall volume constraint. This follows the approach used in the analysis of the inviscid drop, Part 1. In contrast to Part 1, a no-slip boundary condition must be satisfied on the solid support. To that end, a set of modified boundary conditions (3.12), valid on the full interface, are introduced. An indicator function (3.13) is used to 'turn on' the solid support. With the modified boundary conditions, one can derive the operator equations (3.20) and (3.26). Reduction of the operator equation to a set of linear algebraic equations could use various functions as a basis. We choose Legendre polynomials since this allows one to proceed further with closed-form expressions. The solvability condition for this matrix equation gives rise to the (nonlinear) characteristic equation for the complex eigenvalue γ^*. The modified boundary conditions and the solution approach presented here are verified against limiting cases in the literature (Prosperetti 1980*b*; Strani & Sabetta 1988).

Eigenvalue solutions are reported as a function of viscosity parameter ϵ for a viscous drop and a bubble in a viscous medium, for selected belt-support positions and extent. The effect of viscosity is seen to be a combination of the extent of no-slip at the solid boundary and internal friction due to relative motion in the bulk. For the bubble, the diffusion of vorticity into the infinite bulk mitigates the influence of the no-slip boundary. The bubble never undergoes a transition from under- to over-damped. On the other hand, for the viscous drop, as ϵ is increased a critical damping ϵ_c is always predicted. Our predictions of critical damping for the drop suffer the same difficulties reported by Strani & Sabetta (1988), most likely due to the inefficiency in capturing viscous structures by the Legendre function basis.

We report that, although internal flow structures change significantly with increasing ϵ, the interface shapes change little. This motivates a 'frozen interface' approximation as a means to estimate the critical damping for the viscous drop. Based on relative error, it provides an estimate of ϵ_c that is within $\sim$10 % of the actual value. Critical damping as it depends on belt geometry is also estimated. Contours over the geometry plane are presented.

This work focuses on axisymmetric interface dynamics of a viscous drop. There also exist shear/rotational wave solutions of the governing equations. These are admitted if one considers an additional vector potential that can generate a radial component of vorticity. Extension to these over-damped motions is given in appendix C.

Acknowledgements

This work was supported by NSF Grant CBET-0653831 and NASA Grant NNX09AI83G.

Appendix A. Modified boundary conditions

The details required to determine $T_n^i(R)$ and $T_n^e(R)$ from the modified boundary conditions (3.12) are given here. For efficiency in presentation, define

$$\widetilde{J}_n \equiv \mathrm{J}_{n+3/2}\left(\left(\gamma^*/\epsilon_i\right)^{1/2}\right), \quad \widetilde{H}_n \equiv \mathrm{H}^{(1)}_{n-1/2}\left(\left(\mu\gamma^*/\epsilon_i\right)^{1/2}\right). \tag{A 1}$$

To begin, apply the definition of the velocity field (2.20) to (3.12*a*) to give

$$T_n^i\left(\frac{1}{\widetilde{J}_n}\right) + T_n^e\left(\frac{1}{\widetilde{H}_n}\right) = -\gamma d_n\left(\frac{2n+1}{n(n+1)}\right). \tag{A 2}$$

Similarly, (2.16*a*), (2.20) and (3.5) are applied to (3.12*b*) yielding

$$\begin{aligned}&\left(\mu_e\left\{T_n^e\left(1+\frac{2}{\widetilde{H}_n}\right)+\gamma d_n\frac{2\,(n+2)}{n+1}\right\}-\mu_i\left\{T_n^i\left(1-\frac{2}{\widetilde{J}_n}\right)+\gamma d_n\frac{2\,(n-1)}{n}\right\}\right)\\ &\quad\times\,(1-\Gamma(x))\,P_n^{(1)}(x)=\mu_i\left(-T_n^i\frac{2}{\widetilde{J}_n}-\gamma d_n\frac{1}{n}\right)\Gamma(x)P_n^{(1)}(x).\end{aligned} \tag{A 3}$$

To isolate T_n^i and T_n^e, recognize that the sum on n is implicit and both sides of (A 3) may be expanded as a series in $P_n^{(1)}(x)$ to give

$$\begin{aligned}&T_n^i\left(\mu_i\frac{L_n}{\widetilde{J}_n}-\mu_i\left(1-\frac{2}{\widetilde{J}_n}\right)(1-L_n)\right)+T_n^e\left(\mu_e\left(1+\frac{2}{\widetilde{H}_n}\right)(1-L_n)\right)\\ &\quad=\gamma d_n\left(2\left(\mu_i\frac{n-1}{n}-\mu_e\frac{n+2}{n+1}\right)(1-L_n)-\mu_i\frac{L_n}{n}\right).\end{aligned} \tag{A 4}$$

Equations (A 2) and (A 4) are solved to give T_n^i and T_n^e as functions of d_n, or equivalently the interface perturbation y.

Appendix B. Immiscible drop operator equation

To derive the operator equation for an immiscible drop, begin by using the scalings (3.18) to recast (3.17) in the form

$$\begin{aligned}&\sum_{n=1}^{\infty}\left\{\left(\left(\rho\frac{1}{n+1}+\frac{1}{n}\right)\gamma^{*^2}+2\,(n-1)\,(n+2)\,(\mu-1)\,\gamma^*\epsilon_i\right)d_n+n\,(n+2)\,\mu\gamma^*\epsilon_i T_n^e\right.\\ &\left.\quad-\,(n-1)\,(n+1)\,\gamma^*\epsilon_i T_n^i\right\}=-\left(\left(1-x^2\right)y_{xx}-2xy_x+2y\right),\end{aligned} \tag{B 1}$$

where T_n^i and T_n^e are determined by solving (A 2) and (A 4) to give

$$T_n^i = \frac{\mu\left(1+\dfrac{2}{\widetilde{H}_n}\right)(1-L_n)\dfrac{2n+1}{n(n+1)} + 2\left((1-L_n)\left(\dfrac{n-1}{n} - \mu\dfrac{n+2}{n+1}\right) - \epsilon_i\dfrac{L_n}{n}\right)\dfrac{1}{\widetilde{H}_n}}{\dfrac{1}{\widetilde{H}_n}\left(\epsilon_i\dfrac{L_n}{\widetilde{J}_n} - \left(1-\dfrac{2}{\widetilde{J}_n}\right)(1-L_n)\right) - \dfrac{1}{\widetilde{J}_n}\left(\mu\left(1+\dfrac{2}{\widetilde{H}_n}\right)(1-L_n)\right)} d_n \tag{B 2}$$

and

$$T_n^e = \frac{\left(\left(1-\dfrac{2}{\widetilde{J}_n}\right)(1-L_n) - \epsilon_i\dfrac{L_n}{\widetilde{J}_n}\right)\dfrac{2n+1}{n(n+1)} - \left(2\left(\dfrac{n-1}{n} - \mu\dfrac{n+2}{n+1}\right)(1-L_n) - \epsilon_i\dfrac{L_n}{n}\right)\dfrac{1}{\widetilde{J}_n}}{\dfrac{1}{\widetilde{H}_n}\left(\epsilon_i\dfrac{L_n}{\widetilde{J}_n} - \left(1-\dfrac{2}{\widetilde{J}_n}\right)(1-L_n)\right) - \dfrac{1}{\widetilde{J}_n}\left(\mu\left(1+\dfrac{2}{\widetilde{H}_n}\right)(1-L_n)\right)} d_n. \tag{B 3}$$

Equations (B 2) and (B 3) may be substituted into (B 1) to produce an integro-differential operator equation for an immiscible drop with material parameters ρ, μ and ϵ_i.

Appendix C. Rotational wave solution of the viscous drop under the spherical-belt constraint

Previously, the assumption was made that the vorticity could be written in the form (2.17) using a properly chosen vector potential $\boldsymbol{B}$. This assumption gave rise to solutions with non-trivial radial velocities at the interface and equivalently shape oscillations. To derive the rotational wave solutions, one introduces a vector potential $\boldsymbol{A}$ that generates a radial component of vorticity (Chandrasekhar 1961),

$$\boldsymbol{\omega} = \nabla \times \nabla \times \boldsymbol{A}, \quad \boldsymbol{A} = A(r,\theta)\boldsymbol{e_r}. \tag{C 1}$$

This class of solution does not have a radial component to its velocity field, but rather tangential velocities. As with the other field quantities, $A(r,\theta)$ can be expanded as

$$A(r,\theta) = \sum_{n=1}^{\infty} S_n(r) P_n(\cos\theta). \tag{C 2}$$

Substitution of the vector potential (C 1) into the vorticity equation (2.10*c*) gives

$$\frac{\mu}{\rho}\frac{\mathrm{d}^2 S_n}{\mathrm{d}r^2} + \gamma S_n - \frac{\mu}{\rho}\frac{n\,(n+1)}{r^2} S_n = 0, \tag{C 3}$$

whose general solution is written as

$$S_n^i(r) = \left(\frac{r}{R}\right)^{1/2} S_n^i(R)\frac{\mathrm{J}_{n+1/2}\left(z^i\right)}{\mathrm{J}_{n+1/2}\left(Z^i\right)}, \quad S_n^e(r) = \left(\frac{r}{R}\right)^{1/2} S_n^e(R)\frac{\mathrm{H}^{(1)}_{n+1/2}\left(z^e\right)}{\mathrm{H}^{(1)}_{n+1/2}\left(Z^e\right)} \tag{C 4}$$

with

$$z^{i,e} \equiv r\left(\gamma\frac{\rho_{i,e}}{\mu_{i,e}}\right)^{1/2}, \quad Z^{i,e} \equiv R\left(\gamma\frac{\rho_{i,e}}{\mu_{i,e}}\right)^{1/2}. \tag{C 5}$$

The remaining unknowns $S_n^i(R), S_n^e(R)$ are determined from the shear boundary conditions

$$v_\varphi^i = v_\varphi^e\left[\partial D_1^f, \partial D_2^f\right], \tag{C 6a}$$

$$\tau_{r\varphi}^i = \tau_{r\varphi}^e\left[\partial D_1^f, \partial D_2^f\right], \tag{C 6b}$$

$$v_\varphi^i = v_\varphi^e = 0\,[\partial D^s]. \tag{C 6c}$$

As before, one can use the indicator function to transform (C6) into a uniform set of boundary conditions,

$$v^i_\varphi|_{r=R} = v^e_\varphi|_{r=R}, \tag{C 7a}$$

$$\left(\tau^i_{r\varphi} - \tau^e_{r\varphi}\right)|_{r=R}\,(1 - \Gamma\,(x, \zeta_1, \zeta_2)) = C\Gamma\,(x, \zeta_1, \zeta_2)\, v^i_\varphi|_{r=R}, \tag{C 7b}$$

valid on the entire interface. The relations

$$v_\varphi = -\frac{1}{r}\frac{\mathrm{d}P_n}{\mathrm{d}\theta}S_n(r), \qquad \tau_{r\varphi} = \mu\left(\frac{2}{r^2}S_n(r) - \frac{1}{r}\frac{\mathrm{d}S_n}{\mathrm{d}r}\right)\frac{\mathrm{d}P_n}{\mathrm{d}\theta}, \tag{C 8}$$

are applied to the modified boundary conditions (C7) to generate the characteristic equation,

$$\mu \mathrm{H}_{n+1/2}\,(X^e) - \mathrm{J}_{n+1/2}\left(X^i\right) = (n+2)\,(\mu - 1) + (1-\mu)\,\frac{L_n}{1-L_n}, \tag{C 9}$$

that determines the growth rate of the rotational waves. Here the following definitions have been used:

$$X^i \equiv (\gamma^*/\epsilon_i)^{1/2}, \tag{C 10a}$$

$$X^e \equiv (\mu\gamma^*/\epsilon_i)^{1/2}, \tag{C 10b}$$

$$L_n \equiv \left(\int_{-1}^{1}\left(P^{(1)}_n(x)\right)^2 \Gamma(x, \zeta_1, \zeta_2)\,\mathrm{d}x\right)\left(\frac{2n+1}{2}\frac{(n-1)!}{(n+1)!}\right). \tag{C 10c}$$

REFERENCES

ARFKEN, G. B. & WEBER, H. J. 2001 *Mathematical Methods for Physicists*. Harcourt Academic Press.

BASARAN, O. 1992 Nonlinear oscillations of viscous liquid drops. *J. Fluid Mech.* **241**, 169–198.

BASARAN, O. & DEPAOLI, D. 1994 Nonlinear oscillations of pendant drops. *Phys. Fluids* **6**, 2923–2943.

BATCHELOR, G. K. 1967 *An Introduction to Fluid Dynamics*. Cambridge University Press.

BAUER, H. F. & CHIBA, M. 2004 Oscillations of captured spherical drop of frictionless liquid. *J. Sound Vib.* **274**, 725–746.

BAUER, H. F. & CHIBA, M. 2005 Oscillations of captured spherical drop of viscous liquid. *J. Sound Vib.* **285**, 51–71.

BHANDAR, A. S. & STEEN, P. H. 2005 Liquid-bridge mediated droplet switch: a tristable capillary system. *Phys. Fluids* **17**, 127107.

BISCH, C., LASEK, A. & RODOT, H. 1982 Compartement hydrodynamique de volumes liquides spheriques semi-libres en apesanteur simulee. *J. Mec. Theor. Appl.* **1**, 165–184.

BOSTWICK, J. B. & STEEN, P. H. 2009 Capillary oscillations of a constrained liquid drop. *Phys. Fluids* **21**, 032108.

BOSTWICK, J. B. & STEEN, P. H. 2010 Stability of constrained cylindrical interfaces and the torus lift of Plateau–Rayleigh. *J. Fluid Mech.* **647**, 201–219.

BOSTWICK, J. B. & STEEN, P. H. 2013 Coupled oscillations of deformable spherical-cap droplets. Part 1. Inviscid motions. *J. Fluid Mech* **714**, 312–335.

CHANDRASEKHAR, S. 1961 *Hydrodynamic and Hydromagnetic Stability*. Oxford University Press.

DAVIS, S. H. 1980 Moving contact lines and rivulet instabilities. Part 1. The static rivulet. *J. Fluid Mech.* **98**, 225–242.

HIRSA, A. H., LÓPEZ, C. A., LAYTIN, M. A., VOGEL, M. J. & STEEN, P. H. 2005 Low-dissipation capillary switches at small scales. *Appl. Phys. Lett.* **86**, 014106.

JAMES, A., SMITH, M. K. & GLEZER, A. 2003*a* Vibration-induced drop atomization and the numerical simulation of low-frequency single-droplet ejection. *J. Fluid Mech.* **476**, 29–62.

JAMES, A., VUKASINOVIC, B., SMITH, M. K. & GLEZER, A. 2003*b* Vibration-induced drop atomization and bursting. *J. Fluid Mech.* **476**, 1–28.

LAMB, H. 1932 *Hydrodynamics*. Cambridge University Press.

LÓPEZ, C. A. & HIRSA, A. H. 2008 Fast focusing using a pinned-contact liquid lens. *Nat. Photonics 2* **9**, 610–613.

LÓPEZ, C. A., LEE, C. C. & HIRSA, A. H. 2005 Electrochemically activated adaptive liquid lens. *Appl. Phys. Lett.* **87**, 134102.

MACROBERT, T. M. 1967 *Spherical Harmonics*. Pergamon.

MALOUIN, B. A., VOGEL, M. J. & HIRSA, A. H. 2010 Electromagnetic control of coupled droplets. *Appl. Phys. Lett.* **96**, 214104.

MAXWELL, J. 1898 *Encylopedia Britannica*, 9th edn. Adam and Charles Black.

MILLER, C. A. & SCRIVEN, L. E. 1968 The oscillations of a fluid droplet immersed in another fluid. *J. Fluid Mech.* **32**, 417–435.

OLLES, J. D., VOGEL, M. J., MALOUIN, B. A. & HIRSA, A. H. 2011 Axisymmetric oscillation modes of a double droplet system. *Opt. Express* **19**, 19399–19406.

PADRINO, J. C., FUNADA, T. & JOSEPH, D. D. 2007 Purely irrotational theories for the viscous effects on the oscillations of drops and bubbles. *Intl J. Multiphase Flow* **34**, 61–75.

PROSPERETTI, A. 1980*a* Free oscillations of drops and bubbles: the initial-value problem. *J. Fluid Mech.* **100**, 333–347.

PROSPERETTI, A. 1980*b* Normal-mode analysis for the oscillations of a viscous liquid drop in an immiscible liquid. *J. Méc.* **19**, 149–182.

PROSPERETTI, A. 1980*c* Viscous effects on perturbed spherical flows. *Q. J. Appl. Maths* **34**, 339–352.

RAMALINGAM, S. K. & BASARAN, O. A. 2010 Axisymmetric oscillation modes of a double droplet system. *Phys. Fluids* **22**, 112111.

RAYLEIGH, LORD 1879 On the capillary phenomenon of jets. *Proc. R. Soc. Lond.* **29**, 71–97.

REID, W. H. 1960 The oscillations of a viscous liquid drop. *Q. J. Appl. Maths* **18**, 86–89.

RODOT, H. & BISCH, C. 1984 Oscillations de volumes liquides semi-libres en microgravite-experience es326 dans spacelab 1. *5th European Symp. on Material Sciences under Microgravity, Paper* ESA SP-222, pp. 23–29.

RODOT, H., BISCH, C. & LASEK, A. 1979 Zero-gravity simulation of liquids in contact with a solid surface. *Acta. Astronaut* **6**, 1083–1092.

SEGNER, J. A. 1751 *Comment. Soc. Reg. Goetting*.

SLATER, D. M., LÓPEZ, C. A., HIRSA, A. H. & STEEN, P. H. 2008 Chaotic motions of a forced droplet-droplet oscillator. *Phys. Fluids* **20**, 092107.

SMITH, W. R. 2010 Modulation equations for strongly nonlinear oscillations of an incompressible viscous drop. *J. Fluid Mech.* **654**, 141–159.

STRANI, M. & SABETTA, F. 1984 Free vibrations of a drop in partial contact with a solid support. *J. Fluid Mech.* **141**, 233–247.

STRANI, M. & SABETTA, F. 1988 Viscous oscillations of a supported drop in an immiscible fluid. *J. Fluid Mech.* **189**, 397–421.

THEISEN, E. A., VOGEL, M. J., HIRSA, C. A., LÓPEZ, A. H. & STEEN, P. H. 2007 Capillary dynamics of coupled spherical-cap droplets. *J. Fluid Mech.* **580**, 495–505.

TRINH, E. & WANG, T. G. 1982 Large-amplitude free and driven drop-shape oscillation: experimental results. *J. Fluid Mech.* **122**, 315–338.

TRINH, E., ZWERN, A. & WANG, T. G. 1982 An experimental study of small-amplitude drop oscillations in immiscible liquid systems. *J. Fluid Mech.* **115**, 453–474.

VOGEL, M. J., EHRHARD, P. & STEEN, P. H. 2005 The electroosmotic droplet switch: Countering capillarity with electrokinetics. *Proc. Natl Acad. Sci.* **102**, 11974–11979.

VOGEL, M. J. & STEEN, P. H. 2010 Capillarity-based switchable adhesion. *Proc. Natl Acad. Sci.* **107**, 3377–3381.

VUKASINOVIC, B., SMITH, M. K. & GLEZER, A. 2007 Dynamics of a sessile drop in forced vibration. *J. Fluid Mech.* **587**, 395–423.

WANG, T. G., ANILKUMAR, A. V. & LEE, C. P. 1996 Oscillations of liquid drops : results from usml-1 experiments in space. *J. Fluid Mech.* **308**, 1–14.